23rd ABCM International Congress of Mechanical Engineering
December 6-11, 2015, Rio de Janeiro, RJ, Brazil

NONLINEAR DYNAMICS OF SMA OSCILLATOR USING A CONSTITUTIVE MODEL WITH INTERNAL CONSTRAINTS

Larissa Maciel da Fonseca [1]
Alberto Paiva [1]
Marcelo Amorim Savi [2]

[1] Universidade Federal Fluminense
Volta Redonda School of Engineering
Department of Mechanical Engineering
420 Trabalhadores Av.
Volta Redonda – RJ – Brazil – 27.255-250
larissamaciel.lah@gmail.com; paiva.ufrj@gmail.com (corresponding author)

[2] Universidade Federal do Rio de Janeiro
COPPE – Department of Mechanical Engineering
Rio de Janeiro – RJ – Brazil – 21.945.970 – P.O. Box 68.503
savi@mecanica.ufrj.br

Abstract. *The amazing properties of Shape Memory Alloys (SMA) have been inspiring many smart structures applications. The mechanical force provided by this stuff comprises hystereses due to either temperature or stress-induced phase transformations, introducing an intrinsic nonlinearity on the mathematical formulation. A consistent constitutive model able to capture the general thermomechanical behavior of SMAs is required in order to adequately describe some specific dynamical features. This contribution deals with the dynamical modeling and numerical simulation of a one-degree of freedom oscillator, including a SMA restoring element, whose constitutive behavior is described through an internal constraints model present in the literature. Numerical simulations are carried out, using the fourth-order Runge-Kutta method. Numerical results for free vibration attest the presence of multiple equilibrium points, indicating system's sensibility to initial conditions; while, for harmonically forced vibrations, trajectories on state space and Poincare sections for different qualitative behaviors ranging from periodic to chaotic are obtained, based on a bifurcation diagram varying the forcing amplitude.*

Keywords: *Shape memory alloy, smart structures, numerical simulation.*

1. INTRODUCTION

Shape Memory Alloys (**SMA**) dynamical applications have become a point of great interest not only in the academic field but also among manufacturing industries. The adaptive feature inherent to this kind of device, due to its hysteretic behavior, enables several designing configurations based on either pseudoelastic behavior or Shape Memory Effect (**SME**). Regarding dynamical applications, intelligent structures using **SMA** may vary from undersea and in-land robots to adaptive bearings to control vibrations in rotating machines and have been discussed by several authors in the literature, such as: Williams et al. (2002); Savi & Pacheco (2002); Lagoudas et al. (2004); Savi et al. (2011); Silva et al. (2013), among others. In most of these cases, **SMA**s are used as sensors. For this kind of task, **SMA**s' outstanding advantage consists of their high specific actuation energy density (work output per unit mass), which propitiates high strain level recovery (or huge restoring forces, while constraining their displacement). On the other hand, the main drawback of **SMA** use is the actuation (usually by temperature) feedback lag – especially when compared to other kinds of actuation such as electric or magnetic. This response delay has a meaningful influence over high-frequency dynamical applications. Despite of the fact that the martensitic transformations that **SMA**s undergo are non-diffusive, there is a heat flux associated to these transformations (being the direct one exothermic, while the reverse one is endothermic), due to the interaction of the **SMA** element with the surrounding environment. In a high-frequency oscillating dynamical system, there is a high mechanical loading/unloading rate. Thus, there is no due time for the **SMA** element to perform the necessary heat exchange with the surrounding environment. As a consequence, a change in temperature of the **SMA** sample takes place, affecting **SMA** mechanical properties and, consequently, affecting the system dynamics (Seelecke, 2002; Bernardini & Rega, 2005). For more details about **SMA** applications, please refer to the following references: Wayman (1980); Duerig *et al*. (1990); Birman (1997); Otsuka & Wayman (1998); Paiva and Savi (2006); Lagoudas (2008), among others.

A point of great importance, during mechanical modeling of **SMA** systems, is to use a consistent constitutive model able to capture all the potentialities of this class of materials. Within this context, the target of this paper is to formulate a mechanical model and carry out numerical simulations for a discrete **SMA** one-degree of freedom oscillator, considering the internal constraints constitutive model proposed by Savi and co-workers, which describes a wide variety of phenomena. The numerical solution of the whole set of equations involves the Operator Split technique, where the dynamical problem is solved apart from the constitutive problem. The resulting dynamical ordinary differential equations' system is solved using a fourth-order *Runge–Kutta* scheme, while the constitutive equations use the implicit *Euler* method combined with an orthogonal projection algorithm. An iterative procedure is responsible for the state variables' convergence. Concerning the numerical results, firstly, for free undamped vibration, equilibrium points are identified at different temperatures, in order to help interpreting the further harmonically forced vibration results, which are evaluated through trajectories on state space and Poincare sections for different qualitative behaviors ranging from periodic to chaotic. These situations are identified from a bifurcation diagram varying the forcing amplitude.

2. MATHEMATICAL MODELING

This section aims to develop the coupled (constitutive + dynamical) system of equations to describe the **SMA** oscillator behavior. It contains two subsections – the first one present the constitutive modelling and the second one incorporates this constitutive model into the dynamical model, besides a brief discussion about the numerical procedure for computational implementation.

2.1 Constitutive Modeling

This subsection refers to the constitutive model used to describe the **SMA** thermomechanical behavior. The formulation adopted herein is the one proposed by Savi and co-workers, which has been adapted from Fremond's original model with internal constraints (Fremond, 1987). A one-dimensional simplified version of Savi's three-dimensional model (Oliveira et al. 2010) is considered in the present work, based on the article proposed by Paiva et al. (2005), discarding the effects of plasticity and tension-compression asymmetry. This constitutive theory takes into account four internal variables β_1, β_2, β_3 and β_4 representing the respective macroscopic volumetric fractions related to: two variants of detwinned martensite (**M+** associated to tension and **M–** associated to compression); austenite (**A**) and twinned martensite (**M**) induced by temperature. Obviously, it is possible to express one of the internal state variables as a function of the other three. Choosing to eliminate twinned martensite (**M**), i.e.: $\beta_4 = 1 - \beta_1 - \beta_2 - \beta_3$, the following set of constitutive equations arises:

Chart 1. Mathematical equations for Savi's and co-workers constitutive model (Paiva et al. 2005).

STRESS–STRAIN–TEMPERATURE CONSTITUTIVE RELATION

$$\sigma = E\,\varepsilon + \left(\alpha + E\alpha_h\right)(\beta_2 - \beta_1) - \Theta\,(T - T_0)$$

COMPLEMENTARY PHASE TRANSFORMATION EVOLUTION EQUATIONS

$$\dot{\beta}_1 = \frac{1}{\eta_M}\left\{\alpha\varepsilon + \Lambda_M + \left(2\alpha_h\alpha + E\alpha_h^2\right)(\beta_2 - \beta_1) + \alpha_h\left[E\varepsilon - \Theta(T - T_0)\right] - \partial_{\beta_1} J_\pi\right\} - \partial_{\dot{\beta}_1} J_\chi$$

$$\dot{\beta}_2 = \frac{1}{\eta_M}\left\{-\alpha\varepsilon + \Lambda_M - \left(2\alpha_h\alpha + E\alpha_h^2\right)(\beta_2 - \beta_1) - \alpha_h\left[E\varepsilon - \Theta(T - T_0)\right] - \partial_{\beta_2} J_\pi\right\} - \partial_{\dot{\beta}_2} J_\chi$$

$$\dot{\beta}_3 = \frac{1}{\eta_A}\left\{-\frac{1}{2}(E_A - E_M)\left[\varepsilon + \alpha_h(\beta_2 - \beta_1)\right]^2 + \Lambda_A + (\Theta_A - \Theta_M)(T - T_0)\left[\varepsilon + \alpha_h(\beta_2 - \beta_1)\right] - \partial_{\beta_3} J_\pi\right\} - \partial_{\dot{\beta}_3} J_\chi$$

With respect to the equations presented in Chart 1, the state variables are: the axial stress σ; the axial strain ε and the absolute temperature T, besides the internal variables $\beta_{( )}$, (with: i = 1,2,3) already defined.

Concerning the model parameters, subscripts "*A*" and "*M*" denotes physical/mechanical properties associated to austenite and martensite, respectively, where: $E_{( )}$ are the elastic moduli; $\Theta_{( )}$ are related to thermal expansion coefficient; $\Lambda_{( )}$ are temperature-dependent parameters responsible for beginning critical stress for direct transformations, given by: $\Lambda_M = -L_0^M + \left(L^M / T_M\right)(T - T_M)$ and $\Lambda_A = -L_0^A + \left(L^A / T_M\right)(T - T_M)$; $\eta_{( )}$ control the intrinsic **SMA** dissipation and may assume different values for loading $\eta^L_{( )}$ and unloading $\eta^U_{( )}$ conditions; α_h is a phase transformation parameter that controls the hysteresis loop width and is related to the maximum residual strain ε_R through: $\alpha_h = \varepsilon_R - (\alpha / E_M)$, while the parameter α controls the hysteresis loop height and T_0 is a reference temperature for null strain. Besides, the parameters E and Θ are assumed as linear combinations of their respective austenitic and martensitic values, i.e.: $E(\beta_3) = E_M - \beta_3(E_M - E_A)$ and $\Theta(\beta_3) = \Theta_M - \beta_3(\Theta_M - \Theta_A)$.

Moreover, $J_\pi(\beta_i)$ is the indicator function with respect to the convex set π that establishes the physical requirement for different phases' coexistence, defined as: $\pi = \left\{ \beta_i \in \Re \mid 0 \le \beta_i \le 1;\ \beta_1 + \beta_2 + \beta_3 \le 1 \right\}$ for (i = 1,2,3), whereas $\partial_{\beta_i} J_\pi$ are the subdifferentials of the indicator function J_π with respect to β_i (Rockafeller, 1970). Analogously, $J_\chi\left(\dot{\beta}_i\right)$ is the indicator function associated to the convex set χ that provides constraints to enable subloops description.

2.2 Constitutive–Dynamical Model Coupling

This subsection is devoted to introduce the constitutive equations presented in the previous subsection into the dynamical model. Aiming an optimized numerical implementation, the resulting set of ordinary differential equations of motion is put in a dimensionless form. After that, an iterative numerical procedure, involving the fourth-order Runge-Kutta method and an orthogonal projection algorithm (used to solve the **SMA** constitutive evolution equations for β_i where: i = 1,2,3), is scrutinized.

Figure 1 presents the physical model for the **SMA** oscillator. Figure 1(a) shows the discrete one-degree of freedom physical model itself, while Fig. 2(b) illustrates the associated free-body diagram. In this layout, m represents the mass, which undergoes a linear displacement $u(t)$ and is submitted to an external excitation $F(t)$; while c is the damping coefficient. Concerning the **SMA** restoring element, it is considered as a bar submitted to tension-compression loadings with crossectional area A_{SMA} and lenght L_{SMA}.

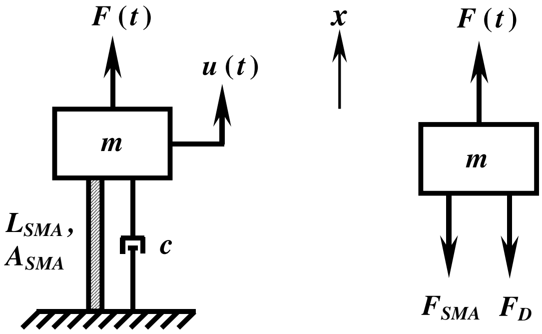

Figure 1. Physical model for the **SMA** oscillator. (a) Physical model; (b) Free-body diagram.

According to the free-body diagram of Fig. 1(b), considering that the body force is canceled out with the static pre-tension in the restoring element, Newton's equation of motion for "x" direction provides:

$$-F_{SMA} - F_D + F(t) = m\ddot{u} \tag{1}$$

The damping force F_D is considered linear: $F_D = c\,\dot{u}$; the external excitation is considered harmonic: $F(t) = F\cos(\Omega t)$, while the **SMA** restoring force F_{SMA} is given by: $F_{SMA} = \sigma A_{SMA}$, where σ is the uniaxial stress given by the stress-strain-temperature relation presented in Chart 1. Thus, substituting all these information in Eq. (1), the equation of motion becomes:

$$-E\,A_{SMA}\left[\varepsilon + \alpha_h(\beta_2 - \beta_1)\right] - \alpha\,A_{SMA}(\beta_2 - \beta_1) + \Theta\,A_{SMA}(T - T_0) - c\,\dot{u} + F\cos(\Omega t) = m\ddot{u} \tag{2}$$

Under infinitesimal strains assumption, the instantaneous total uniaxial strain may be assumed as: $\varepsilon = u / L_{SMA}$ and, thus, the equation of motion remains in the general form as follows:

$$m\ddot{u} + c\,\dot{u} + \frac{E\,A_{SMA}}{L_{SMA}}u + A_{SMA}\left[(\alpha + E\alpha_h)(\beta_2 - \beta_1) - \Theta(T - T_0)\right] = F\cos(\Omega t) \tag{3}$$

To obtain the dimensionless differential equations of motion, consider the new variables: $\tau = \omega t$ as the new independent variable, where ω is an angular frequency concerning a reference value; $U = u / L_{SMA}$ is the new dimensionless displacement; while $\theta = T / T_M$ is the new variable for dimensionless temperature.

At this point, the original variable $u(t)$ and its derivatives are substitued for the new dimensionless variable $U(\tau)$, and its derivatives $U'(\tau)$ and $U''(\tau)$, where: $U' = dU/d\tau$. Therefore, regarding that: $U = U(\tau(t))$, by applying the chain's rule, $\dot{u} = L_{SMA}\,\omega U'$ and $\ddot{u} = L_{SMA}\,\omega^2 U''$. Moreover, dividing Eq. (3) by the factor $m L_{SMA}\,\omega^2$ and performing the necessary algebraic procedures, finally, the following second-order ordinary differential equation arises:

$$U'' + \xi U' + \gamma U + \left(\bar{\alpha} + \gamma\,\alpha_h\right)(\beta_2 - \beta_1) - \bar{\Theta}\,(\theta - \theta_0) = \delta \cos\left(\bar{\omega}\tau\right) \tag{4}$$

Concerning the new dimensionless parameters of Eq. (4), adopting the reference frequency as: $\omega = \sqrt{E_M A_{SMA} / m L_{SMA}}$, they are related to the original ones as follows:

$$\xi = \frac{c}{m\omega};\quad \gamma = \frac{E A_{SMA}}{m L_{SMA}\,\omega^2} = \frac{E}{E_M};\quad \bar{\alpha} = \frac{\alpha A}{m L_{SMA}\,\omega^2} = \frac{\alpha\gamma}{E} = \frac{\alpha}{E_M};\quad \bar{\Theta} = \frac{\Theta A T_0}{m L_{SMA}\,\omega^2} = \frac{\gamma\,\Theta\,T_M}{E} = \frac{\Theta\,T_M}{E_M};$$
$$\theta_0 = \frac{T_0}{T_M};\quad \delta = \frac{F}{m L_{SMA}\,\omega^2} = \frac{\gamma F}{E A} = \frac{F}{E_M A_{SMA}};\quad \bar{\omega} = \frac{\Omega}{\omega} \tag{5}$$

It is worthwhile to notice that the parameters ξ, δ and $\bar{\omega}$ may be directly defined, while the parameters γ, $\bar{\alpha}$, $\bar{\Theta}$ and θ_0 should be calculated from the constitutive model parameters, in such a way that $\bar{\alpha}$ and θ_0 are constant parameters, while γ and $\bar{\Theta}$ vary with time, since they depend upon the parameters E and Θ, respectively, that, in turn, depends on the internal variable β_3, according to the previous definitions: $E = E_M - \beta_3(E_M - E_A)$ and $\Theta = \Theta_M - \beta_3(\Theta_M - \Theta_A)$.

For the purpose of numerical implementation via fourth-order Runge-Kutta method, it is necessary to convert the dimensionless second-order ordinary differential equation (Eq. 4) into a first-order ordinary differential equations' set. Hence, consider a new variables' change, such that: $U = x$; $U' = y$, where the new derivatives denoted by $(\,^\bullet\,)$ correspond to $(\,^\bullet\,) = d(\ )/d\tau$. Finally, the dynamical governing differential equations in their ultimate form are given by:

$$\begin{cases} \overset{\bullet}{x} = y \\ \overset{\bullet}{y} = \delta\cos\left(\bar{\omega}\tau\right) - \gamma U - \xi U' - \left(\bar{\alpha} + \gamma\,\alpha_h\right)(\beta_2 - \beta_1) + \bar{\Theta}\,(\theta - \theta_0) \end{cases} \tag{6}$$

According to the mathematical formulation developed for the coupled constitutive-dynamical problem, the resulting equations provide an ordinary differential equations' system, involving the evolution equations for β_1, β_2 and β_3 present in Chart 1 and the dynamical Eq. (6). The numerical solution of this problem is based upon the *Operator Split* technique (Ortiz *et al.* 1983) that helps to solve the problem in a decoupled way, where the constitutive problem is solved apart from the dynamical problem.

Giving respect to the numerical implementation of the model proposed by Savi and co-workers, the differential evolution equations are integrated using the implicit *Euler* method together with another operator split technique, where the internal variables, calculated without considering the subdifferntials, should obey the internal restrictions defined by both convex sets π and χ that establishes the constraints for phases' coexistence and subloops description, respectively (Paiva et al. 2005). If they do not obey, their values should be orthogonally projected over these domains' surface.

The coupled problem demands an iterative procedure, since the deformation of the **SMA** element is driven by the own oscillator dynamics, through the inertial element displacement U. For this reason, the coupled solution algorithm involves the following steps. Initially, the *Runge-Kutta* sub-routine is used to estimate the dimensionless displacement U, using the present values of the internal variables β_1, β_2 and β_3. This displacement estimative feeds the orthogonal projection sub-routine, which provides updated values for β_1, β_2 and β_3. Within the same time step, with this updated values of the internal variables, the *Runge-Kutta* sub-routine is revisited, providing a new value for the displacement U. This new displacement estimative is used, again, in the orthogonal projection sub-routine, providing re-updated values for β_1, β_2 and β_3. At last, the convergence of the dimensionless displacement U and of the internal variables is verified, by comparing their former estimated values with their new calculated values. If both converge, the algorithm moves forward to the next time step; otherwise, a recursive scheme goes through all these steps again, until they converge.

3. NUMERICAL RESULTS

This section shows some numerical results obtained for free and forced vibrations. Initially, for free undamped vibration, the equilibrium points are identified for different temperatures. Then, for harmonically forced vibration, different behaviors patterns are investigated through trajectories on state space and *Poincare* sections, distinguishing periodic responses from chaotic ones, based on a bifurcation diagram varying the forcing amplitude.. Both the **SMA** parameters and the dynamical parameters used in the numerical simulations are presented in Tabs. 1 and 2, respectively.

Table 1. **SMA** properties and parameters for Savi's and co-workers model.

E_A (GPa)	E_M (GPa)	α (MPa)	ε_R
54	42	260	0.0555
L_0^M (MPa)	L^M (MPa)	L_0^A (MPa)	L^A (MPa)
0.15	415	0.63	185
η_M^L (MPa/s)	η_M^U (MPa/s)	η_A^L (MPa/s)	η_A^U (MPa/s)
10	27	10	27
T_M (K)	T_0 (K)	Θ_A (MPa/K)	Θ_M (MPa/K)
291.4	288.5	0.74	0.17

Table 2. Dynamical system parameters.

ξ	δ	$\bar{\omega}$
5e-6	Varying parameter	1

Figure 2 shows the trajectories on the state space U x U' for free undamped vibration, considering different temperatures. In Fig. 2a, for a high temperature condition with θ = 1.20, three distinct initial conditions are assumed. All them follow a stable (convergent) spiral path associetd to a transient regime, where there is a displacement/velocity amplitude decay, due to hysteretic dissipation induced by phase transformations (remembering there is no damping). During the steady-state, they stabilize into elastic periodic stable orbits, indicating a centre manifold that suggests an oscilation around a single equilibrium point ($U = U' = 0$), associated to the austenitic phase (stable at high temperatures). In Fig. 2b, for a low temperature condition with θ = 0.99, again, for three distinct initial conditions, convergent spiral paths are seen during the transient regime. However, this time, during the steady-state, each of them stabilizes into a different elastic periodic stable orbit, associated with different martensitic variants, as indicated by the subtitles. Obviously, according to the index theory, there are two unstable saddle points between each pair of stable points. This multiple stabilizations attest the system's sensibility to initial conditions. These results help interpreting the further harmonically forced vibration responses.

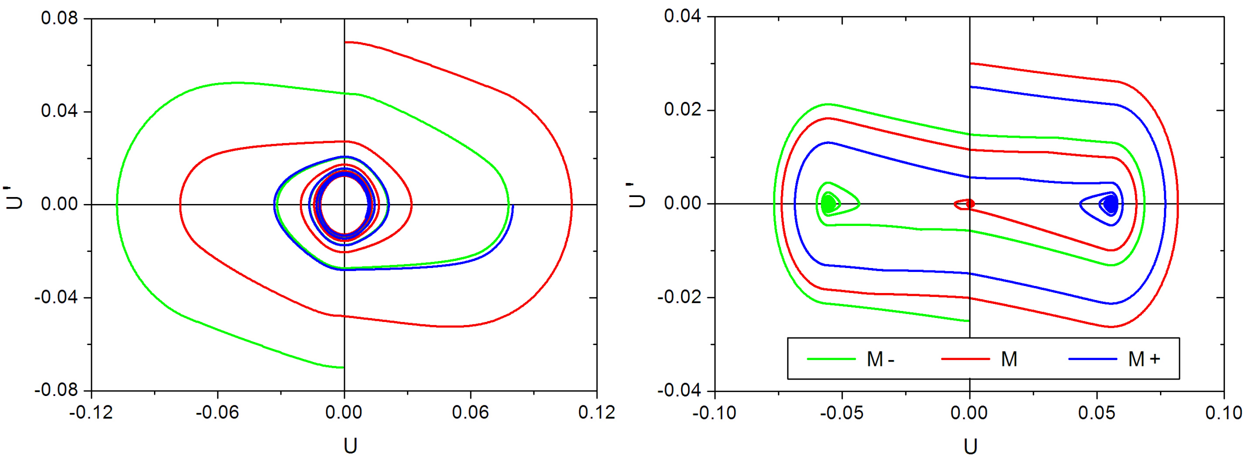

Figure 2. Trajectories on state spaces for different temperatures.
(a) High temperature θ = 1.20; (b) Low temperature θ = 0.99.

Figure 3 shows the bifurcation diagram for the dimensionless displacement U and velocity U' varying with the dimensionless forcing amplitude δ, for a low temperature ($\theta = 0.99$), where two distinct chaotic-like regions can be identified within the analyzed range – being the first one from approximately 0.001 to 0.0025 and the second one from approximately 0.007 to 0.008. Concerning the first region, two typical nonlinear phenomena are recognized, as follows: before this region, there is a bifurcation cascading towards chaos, as shown in both enlarged details for U and U' and, after this region, the chaotic behavior suddenly becomes a period-1 response (for $\delta \cong 0.0025$), characterizing what is known as crisis. In the depicted detail in the main figure, concerning the selected region, U' present a period-2 response as well as U.

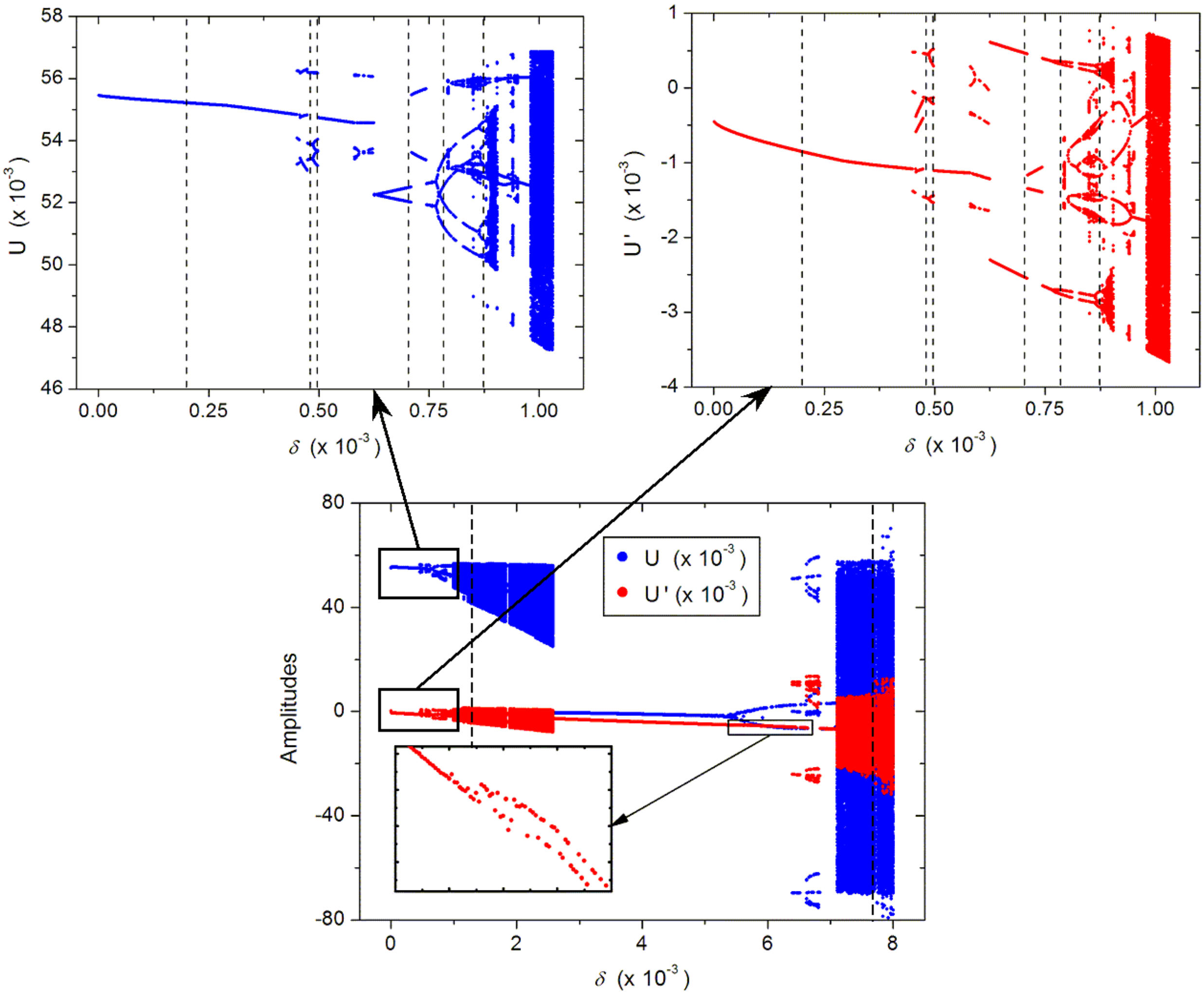

Figure 3. Bifurcation diagrams for U and U' varying the dimensionless forcing amplitude δ.

Based on the bifurcation diagram presented in Fig. 3, eight selected values of the dimensionless forcing amplitude δ are selected (according to the dashed lines present in the main figure and in the depicted details) to illustrate different dynamical patterns (including periodic and chaotic-like situations).

Figure 4 shows the state spaces U x U' for periodic behaviors with different periodicity for the six selected values on both enlarged details. Figure 5 shows the respective *Poincare* sections for these same six selected values, which are: $\delta = 0.0002$; $\delta = 0.000484$; $\delta = 0.0005$; $\delta = 0.0007$; $\delta = 0.0008$ and $\delta = 0.00087$.

Figure 6 shows the *Poincare* sections for the lasting two selected values assigned by the dashed lines in the main figure of Fig. 3. These two values are immersed in the two distinct chaotic-like regions (one for each), i.e.: $\delta = 0.0012$ and $\delta = 0.0078$.

In all phase portraits of Fig. 4, there are closed orbits that characterize periodic behaviors. In Fig. 4a, this closed orbit always follows a single path, indicating a period-1 behavior. The associated *Poincaré* section in Fig. 5a shows a single point, attesting a periodic behavior of period-1.

In the subsequent Figs. 5b, 5c, 5d, 5e and 5f, there are closed orbits in the phase space, indicating periodic behaviors as well; however, for these cases, the orbits follow multiple paths, according to the respective periodicity. The *Poincare* sections showed in Figs. 5b, 5c, 5d, 5e and 5f, for Period-3; Period-6; Period-2; Period-4; and Period-8, respectively, ensure the periodic characteristic of each of these responses.

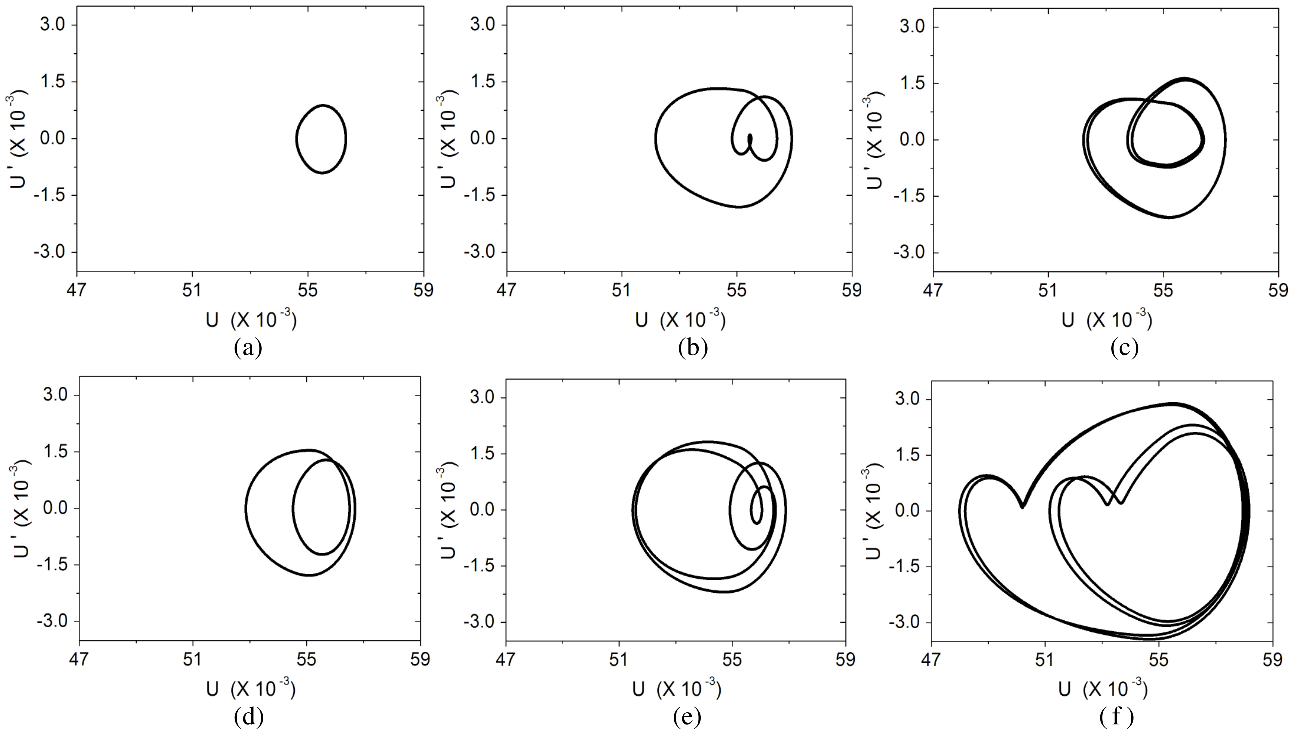

Figure 4. Trajectories on state spaces *U* x *U* '.
(a) Period-1 (δ = 0.0002); (b) Period-3 (δ = 0.000484); (c) Period-6 (δ = 0.0005);
(d) Period-2 (δ = 0.0007); (e) Period-4 (δ = 0.0008); (f) Period-8 (δ = 0.00087).

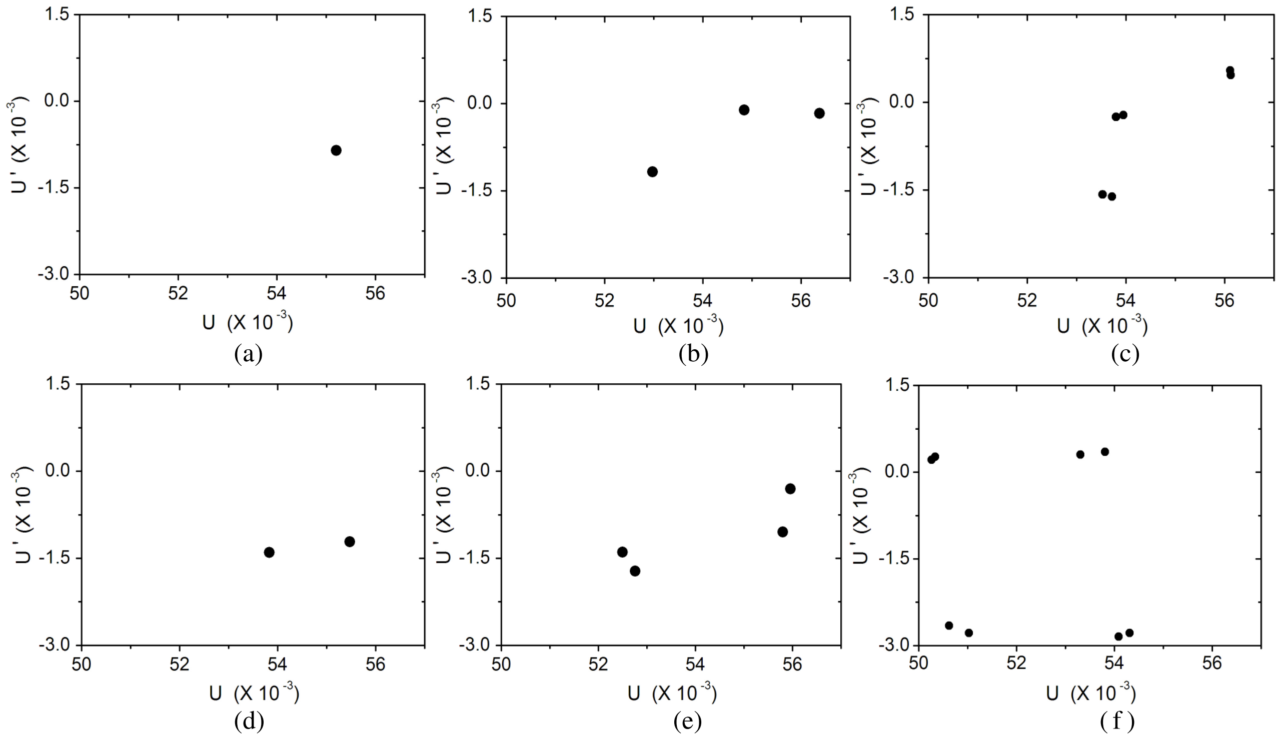

Figure 5. *Poincare* sections for state spaces *U* x *U* '.
(a) Period-1 (δ = 0.0002); (b) Period-3 (δ = 0.000484); (c) Period-6 (δ = 0.0005);
(d) Period-2 (δ = 0.0007); (e) Period-4 (δ = 0.0008); (f) Period-8 (δ = 0.00087).

Figure 6 shows the *Poincare* sections for two chaotic-like responses: δ = 0.0012 and δ = 0.0078. Figs. 6a and 6b show tangled points with a non-regular dynamical response. Nevertheless, lamellar structures are identified, characterizing strange attractors that, in turn, suggest a chaotic behavior. Notice that different chaotic regions provide strange attractors with different structures, modifying the system dynamics.

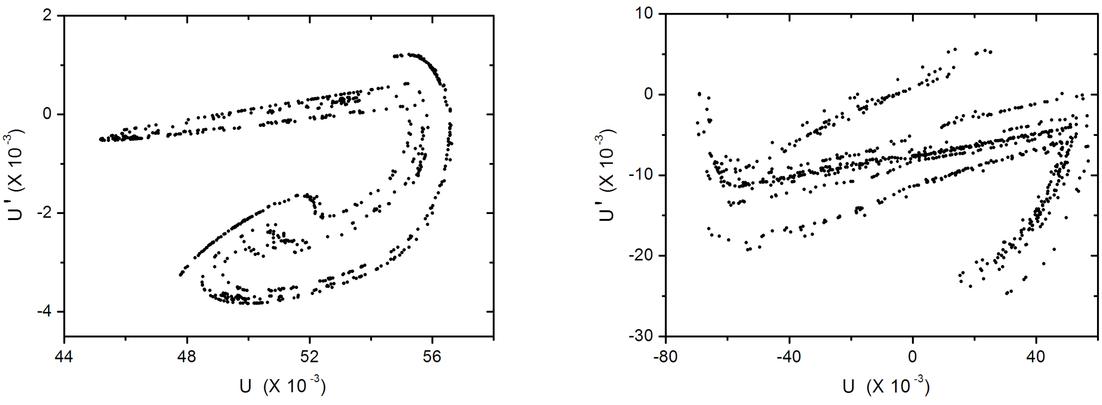

Figure 6. Strange attractors for different chaotic motions. (a) $\delta = 0.0012$; (b) $\delta = 0.0078$.

4. CONCLUDING REMARKS

This paper addresses the nonlinear analysis of a discrete one-degree of freedom oscillator, considering a **SMA** restoring element described by an internal constraints model. Concerning the numerical results, firstly, for free undamped vibration, equilibrium points are identified at different temperatures and sensibility to initial conditions is evaluated. The dynamical investigation of the harmonically forced case is conducted based on the variation of the forcing amplitude. Periodic solutions with different periodicity are illustrated through trajectories on state subspaces and *Poincare* sections. At last, strange attractors are obtained for two distinct chaotic regions of the bifurcation diagram.

5. ACKNOWLEDGEMENTS

The authors would like to acknowledge the support of the Brazilian Research Agencies CNPq, CAPES, FAPERJ as well as INCT-EIE (National Institute of Science and Technology - Smart Structures in Engineering). The acknowledgement applies also to Air Force Office of Scientific Research (AFOSR).

6. REFERENCES

Bernardini, D. & Rega, G.; 2005; “Thermomechanical Modelling, Non-linear Dynamics and Chaos in Shape Memory Oscilators”; *Mathematical and Computer Modelling of Dynamical Systems*; Vol. 11; N. 3; pp. 291–314.

Fremond, M.; 1987; “Matériaux à Mémoire de Forme”; *C.R. Acad. Sc. Paris*; Vol. II, N. 7; pp. 239–244.

Machado, L.G.; Savi, M.A. & Pacheco, P.M.L.C.; 2003; “Nonlinear Dynamics and Chaos in Coupled Shape Memory Oscillators”; *International Journal of Solids and Structures*; Vol. 40; N. 19; pp. 5139–5156.

Machado, L.G.; Savi, M.A. & Pacheco, P.M.L.C.; 2004; “Bifurcations and Crises in a Shape Memory Oscillator”; *Shock and Vibration*; Vol.11; N. 2; pp. 67–80.

Machado, L.G. & Savi, M.A.; 2006; “Free Vibration of Coupled Shape Memory Oscillators: Influence of Temperature Variations”; *SBMAC Bulletin – N. II Series*; Vol. 7; N. 2; pp. 157–170.

Oliveira, S.A.; Savi, M.A. & Kalamkarov, A.L.; 2010; “A Three-Dimensional Constitutive Model for Shape Memory Alloys”; *Archive of Applied Mechanics*; Vol. 80; pp. 1163–1175.

Ortiz, M., Pinsky, P. M. & Taylor, R. L., 1983, Operator Split Methods for the Numerical Solution of the Elastoplastic Dynamic Problem, Computer Methods of Applied Mechanics and Engineering, 39: pp.137-157.

Paiva, A. ; Savi, M. A. ; Braga, A. M. B. ; Pacheco, P. M. C. L. . A Constitutive Model for Shape Memory Alloys Considering Tensile-compressive Asymmetry and Plasticity. *International Journal of Solids and Structures*; Vol. 42; N. 11–12; pp. 3439–3457.

Paiva, A.; Savi, M.A. & Pacheco, P.M.C.L.; 2005; “Modeling Transformation Induced Plasticity in Shape Memory Alloys”; Prceedings of XVIII International Congress of Mechanical Engineering – COBEM 2005 – Ouro Preto – Minas Gerais – Brasil; 8 pp.

Paiva, A. & Savi, M.A.; 2006; “An Overview of Constitutive Models for Shape Memory Alloys”; *Mathematical Problems in Engineering*; Article Id. 56876, Vol. 2006; 30 pp.

Santos, B.C. & Savi, M.A.; 2009; “Nonlinear Dynamics of a Nonsmooth Shape Memory Alloy Oscillator”; *Chaos, Solitons and Fractals*; Vol. 40; pp. 197–209.

Savi, M.A.; Paiva, A. ; Baêta Neves, A.P. & Pacheco, P.M.C.L.; 2002; “Phenomenological Modeling and Numerical Simulation of Shape Memory Alloys: a Thermo-plastic-phase Transformation Coupled Model”; *Journal of Intelligent Material Systems and Structures*; Vol. 13; N. 5; pp. 261–274.

Savi, M.A. & Paiva, A.; 2005; “Describing Internal Subloops Due to Incomplete Phase Transformations in Shape Memory Alloys”; *Archive of Applied Mechanics*; Vol. 74; N. 9; pp. 637–647.

Savi, M.A.; De Paula, A.S. & Lagoudas, D.C.; 2011; “Numerical Investigation of an Adaptive Vibration Absorber Using Shape Memory Alloys” *Journal of Intelligent Material Systems and Structures*; Vol. 22; pp. 67–80,

Seelecke, S.; 2002; “Modeling the Dynamic Behavior of Shape Memory Alloys”; *International Journal of Nonlinear Mechanics*; Vol. 37; N. 8; pp. 1363–1374.

7. RESPONSIBILITY NOTICE

The authors are the only responsible for the printed material included in this paper.